DELPHI Collaboration

DELPHI 2003-005 CONF 628
14 March, 2003

Flavour Independent Neutral Higgs Boson Searches with DELPHI at LEP-2

P. Bambade
LAL, Orsay
M. Boonekamp
CEA, Saclay
G. Borisov
University of Lancaster
M. Stanitzki
Inst. für Exper. Kernphysik, Karlsruhe
E. Graziani
Roma III / INFN
I. van Vulpen
CERN

Preliminary

Abstract

Flavour independent searches for neutral Higgs bosons decaying hadronically are described, using data collected by the DELPHI experiment at LEP in e^+e^- collisions at centre-of-mass energies between 189 and 208 GeV. The collected data-set corresponds to an integrated luminosity of around 610 pb^{-1}. For hZ production the fully hadronic final state, the final state with 2 jets+missing energy and those with two jets+isolated leptons (electrons and muons) were used, while for the hA production process only the fully hadronic channel was used. These searches are more general than the usual standard model or MSSM Higgs boson searches, and lead to results interpretable in a wider range of models. No evidence for Higgs boson production was found and limits on production cross-sections were set for both hZ and hA signal hypotheses as a function of the Higgs boson mass.

Contribution to the Winter Conferences 2003

1 Introduction

The Standard Model Higgs boson decays predominantly into a pair of b-quarks in the mass range accessible to LEP-2. In extensions to the Standard Model (SM), the Higgs boson couplings to quarks might be suppressed. This can occur for example in the general Two Higgs Doublet Model (2HDM)[1] or in the Minimal Supersymmetric Standard Model (MSSM)[2]. Suppressed couplings to b-quarks are also possible in special composite models, in which the dominant Higgs decay channel is the one into gluons[3]. The searches for the SM Higgs boson at LEP strongly rely on the identification of b-quarks to separate possible signal production from most of the background and would therefore have a reduced sensitivity to the final states predicted by such models. To test these models experimentally, DELPHI developed dedicated searches, that are independent of the quark flavour in the Higgs boson decay. Such flavour-independent Higgs searches, only requiring a hadronic decay of the Higgs boson, lead to more model-independent cross section results that can be used to test the predictions given by a wide range of models.

In this paper, two Higgs production processes have been studied: the Higgsstrahlung process, ($e^+e^- \to Z^* \to hZ$) and pair production of the CP-even h and the CP-odd A Higgs boson ($e^+e^- \to Z^* \to hA$), which is predicted in the 2HDM.

The search for hZ production, using the fully hadronic final state, the final state with 2 jets+missing energy and those with two jets+isolated leptons (electrons and muons) is described in section 4. For the hA pair production only the fully hadronic final state has been studied as described in section 5. In section 6 the various analyses are combined to give flavour independent results on production cross sections.

2 General strategy

To ensure flavour independence of our results, care must be taken not to bias our search towards a specific hadronic decay mode of the Higgs boson. When comparing final states with quarks and gluons, two sizeable and competing effects arising from the different hadronization of quarks and gluons had to be considered: the higher multiplicity of gluon jets results on one side in an increased efficiency for the gluonic final state, but also in a worse dijet mass resolution compared to quarks. To achieve sensitivity for Higgs boson production over the full Higgs mass range, dedicated low and high mass anayses were developed for most final states (sensitive roughly below and above 40 GeV/c^2 respectively) and for each final state both Higgs decays into gluons and quarks were evaluated. The procedure for combination into a flavour independent result is described in section 6.

3 Detector, data samples and simulation

The data samples used were collected by DELPHI from 1998 to 2000, and were clustered around seven centre-of-mass energies (see Table 1). A detailed description of the DELPHI detector and the performance of the sub-systems can be found in [4]. For the year 2000 data taking, there was a period, when 1/12 of the main tracking device (TPC) of DELPHI was not operational. The change in sensitivity during this period has been taken into account by using dedicated simulation samples.

year	1998	1999				2000	
$\sqrt{s}$ (GeV)	188.6	191.6	195.5	199.5	201.6	205.0	206.5
$\mathcal{L}$ (pb^{-1})	158	25.9	76.9	84.3	41.1	82.0	142.2

Table 1: *Integrated luminosities collected by the DELPHI detector at various centre-of-mass energies during the period 1998-2000.*

Background samples

Standard Model background events with a two-fermion final state were generated using the KK2F[5] and PYTHIA[6] generators, while for four-fermion final states the WPHACT[7] and EXCALIBUR[8] generators were used. Two-photon final states were generated using PYTHIA and all signal samples were generated using the HZHA[9] generator at mass points as described below.

hZ signal samples and data-sets

In the hZ analysis the data from all seven centre-of-mass energies as listed in Table 1 have been analysed. hZ signal samples have been generated at masses from 40 to 120 GeV/c^2 with a step size of 2.5 GeV/c^2 and the Higgs was made to decay in either $s\bar{s}$ or into a pair of gluons. For fully hadronic final states at Higgs masses below 40 GeV/c^2 simulated hA samples have been used where the A mass was fixed to the mass of the Z boson.

hA signal samples and data-sets

In this analysis all data-sets except those at centre-of-mass energies of 191.6 and 201.6 were analysed. The simulation of the hA production process was done in the range m_h,m_A>4 GeV/c^2 and m_h+m_A<180 GeV/c^2, using a grid of 5 GeV/c^2 if one of the masses was below 30 GeV/c^2 and 10 GeV/c^2 if both were above.

4 hZ channels

For hZ production, most of the analyses used for the search for a hadronically decaying Higgs boson are adapted from different existing analyses already preformed in DELPHI. In most cases, a minimal description of the main ingredients in the analysis is given and a reference is made to the publication where the analysis is described in more detail. The various analyses, targeting the different decay modes of the Z boson and Higgs boson mass ranges are described below.

4.1 Fully hadronic

Higgs masses above 40 GeV/c^2

The probabilistic selection used to analyse the four jet channel in the $e^+e^-\rightarrow ZZ$ production measurement[10] was adapted to test the hypothesis of Higgs boson production independently of the flavour of its decay products. After a hadronic, multi jet preselection, a combined variable was constructed to select the signal at each test mass based on topological information and on the specific invariant mass information, following the

method described in [10]. The b-tagging information was used in the formulation of this variable, but only for jets assigned to the Z boson.

To give an idea of the agreement between observation and expectation, in Table 2 the number of observed events is compared to what is expected from background and signal ($H \rightarrow s\bar{s}$) for a few Higgs boson masses at the value of the cut on P_{Higgs} for which the product of signal efficiency and purity is maximal. Examples of the resulting probability distributions are shown in Figure 1, for Higgs boson masses of 75, 90 and 105 GeV/c^2, respectively, adding the events from all centre-of-mass energies. The dominant background depends on the tested mass: ZZ production dominates the high purity region as expected for the 90 GeV/c^2 mass hypothesis, and QCD processes $q\bar{q}gg$ are generally quite important elsewhere.

The systematic uncertainties are dominated by the uncertainty in the four jet cross-section originating from QCD processes in the simulation [11]. This uncertainty was conservatively taken to be 10% over the full Higgs mass range. The effect of other systematics as evaluated in [10] are negligible compared to this.

M_H (GeV/c^2)	ϵ(hZ)	hZ(ss)	SM(no hZ)	observed
40	31.3	154.6	635.0	659
50	30.1	132.3	522.8	532
60	51.9	197.1	1784.1	1824
70	78.6	249.3	5457.3	5476
80	54.2	136.0	1681.7	1764
90	54.6	96.2	957.4	970
100	47.0	41.1	368.5	372
110	33.9	9.4	87.6	75

Table 2: The number of observed events compared to what is expected from background and signal ($H \rightarrow s\bar{s}$, assuming a SM-like cross section) for a few Higgs boson masses at the value of the cut on P_{Higgs} for which the product of signal efficiency and purity is maximal. Using the combined set of simulated events at all centre-of-mass energies, the statistical uncertainties on both the signal efficiency and background level are below 1%. This also holds for the estimates of efficiencies and background levels for other topologies, as described elsewhere in this note.

Higgs masses below 40 GeV/c^2

At low Higgs masses, fully hadronic events tend to become more three jet-like, since the decay jets of the lighter Higgs boson are not always resolved due to the larger boost. The region of Higgs boson masses below 40 GeV/c^2 has therefore been covered by the three jet hA analysis (described in more detail in section 5.1) where the mass of the A has been fixed to the mass of the Z boson.

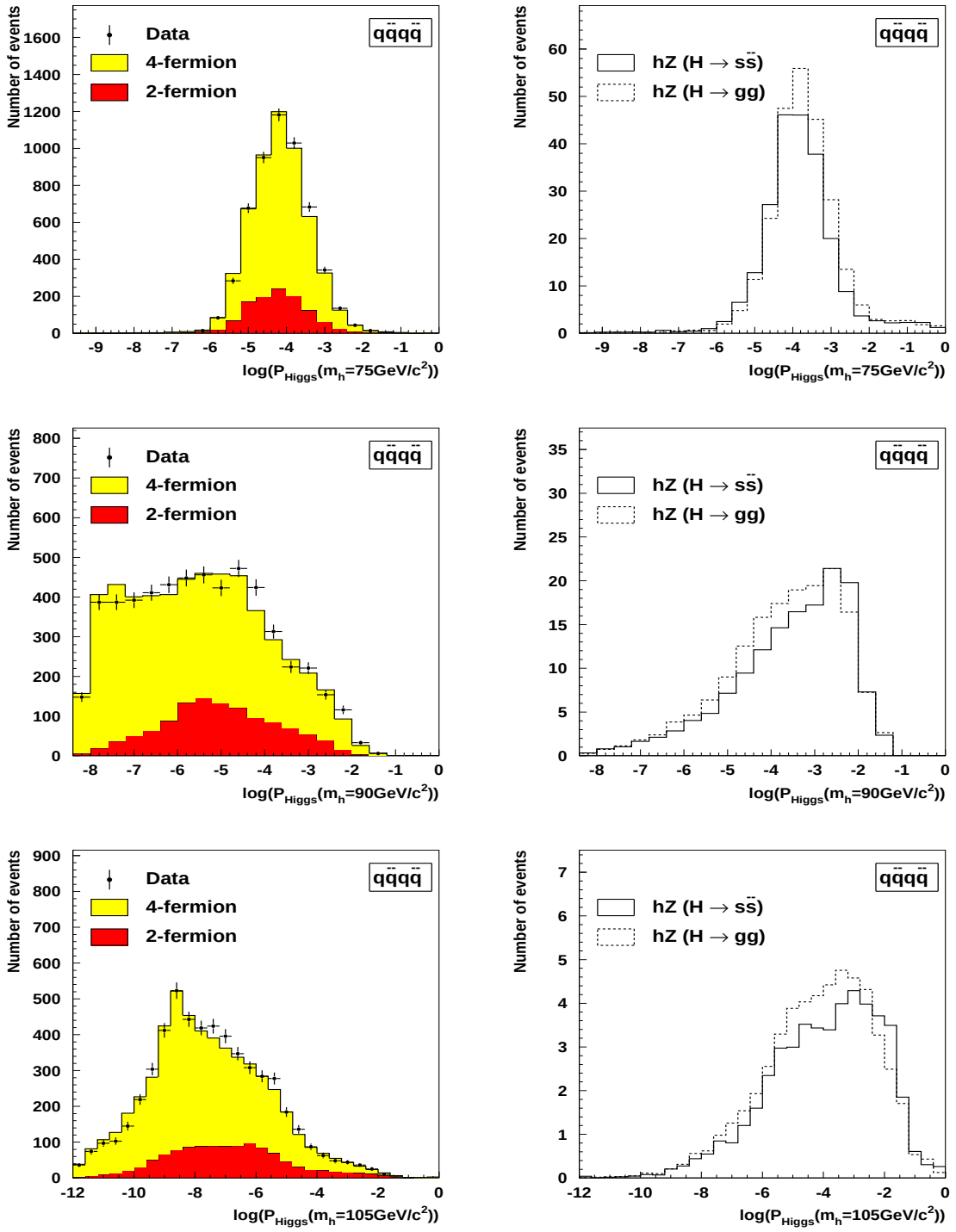

Figure 1: Distributions of the combined Higgs probabilities for the fully hadronic final state, constructed in the hypotheses of hZ production for Higgs boson masses of 75, 90 and 105 GeV/c^2 respectively (from top to bottom). In these distributions, the data from all centre-of-mass energies in 1998, 1999 and 2000 are added. As it has been shown that the P_{Higgs} provides a good estimate of the true probabilities to select events in the corresponding hypotheses, the distributions for different centre-of-mass energies can be added with only limited dilution.

4.2 Two jets and missing energy (High mass case)

This analysis searches for events with two jets and missing energy, compatible with a Z boson decaying into two neutrinos. It follows closely the analysis for invisible Higgs decays with the Z boson decaying hadronically as described in [12]. To obtain a good performance over the whole mass range, three mass windows (low, intermediate and high) were defined, each with a dedicated analysis. The mass windows range from 40 to 67.5 GeV/c^2, from 70 to 90 GeV/c^2 and from 92.5 to 115 GeV/c^2. To reduce background originating from $q\bar{q}\gamma$ and $\gamma\gamma$ processes, a common preselection for all three analyses was applied that is described in detail in [12] together with the jet clustering algorithm. To obtain further discrimination between signal and background events, tail cuts were performed on the variables, that are then used in an Iterative Discriminant Analysis (IDA)[13]. All events containing more than two clearly identified leptons were rejected and to maximise discrimination between signal and background, two IDA steps were performed.

4.2.1 Low mass analyses ($40.0\ \mathrm{GeV/c^2} < m_h < 67.5\ \mathrm{GeV/c^2}$)

In the low mass analysis, twelve variables were used to construct an efficient IDA variable. Most of the variables are in common with the invisible Higgs analysis and are described there [12]. In the IDA were used: the logarithm of the transverse momentum of the event, the visible and the transversed energy, the logarithm of the energy of the least energetic jet in the three-jet configuration, the difference between the Fox-Wolfram[14] momenta H2 and H4, the energy and the momentum of the most isolated particle, acoplanarity and acollinearity, the missing mass and the transverse momentum of any particle in the jet with respect to the nearest jet axis. A two step IDA was used to separate between signal and background and the IDA was also trained over the whole mass range from 40 to 67.5 GeV/c^2. To remain truly flavour independent, the IDA was trained simultaneously on all flavours (using also Higgs decays into heavy quarks: $c\bar{c}$ and $b\bar{b}$), resulting in an comparable performance for all flavours.

4.2.2 Intermediate mass analyses ($70.0\ \mathrm{GeV/c^2} < m_h < 87.5\ \mathrm{GeV/c^2}$)

In the analysis for the intermediate mass range, again twelve variables were used. Because of the different event toplogy, the variable related to the logarithm of the energy of the least energetic jet in the three-jet configuration was replaced by the event b-tag probability for a 2 jet hZ configuration[15]. The IDA was calculated in the same way as in the low mass analyses, except that the mass range for the IDA training now ranged from 70 to 87.5 GeV/c^2.

4.2.3 High mass analyses ($90.0\ \mathrm{GeV/c^2} < m_h < 115\ \mathrm{GeV/c^2}$)

The same 12 variables as in the intermediate mass analyses were also used in the high mass analysis with slightly different tail cuts. The mass range for the training of the IDA was varied for the different centre-of-mass energies, ranging from 92.5 to 97.5 GeV/c^2 for 188.6 GeV data, from 92.5 to 107.5 GeV/c^2 for 191.6 to 201.6 GeV data and finally, from 92.5 to 115 GeV/c^2 for 205 to 206.5 GeV data. This was done to avoid training on off-shell events (beyond the kinematical limit) for the hZ process.

Mass reconstruction and final discriminant variable

The mass of the di-jet system, which corresponds to the mass of the Higgs boson, was calculated with a Z-mass constraint for the missing mass as in [12]. The distribution of the reconstructed Higgs mass for background and signal events is used, for each Higgs mass hypothesis separately, to select candidate events from within a mass window that is optimised to maximize the product of efficiency and purity. To give an idea of the agreement between observation and expectation, at this stage, in Table 3 the number of observed events is compared to what is expected from background and signal ($H \rightarrow s\bar{s}$) for a few Higgs boson masses.

The discriminant variable computed in the second step of the IDA after this selection is used as the variable to compute cross section exclusion limits. The distribution of the IDA variable after the second iteration is shown in Figure 2 for data, background and signal events for three different Higgs mass hypotheses: 75, 90 and 105 GeV/c^2. In this figure, the distributions for all centre-of-mass energies have been combined.

In this topology, the discrimination between signal and background is much better for the gluon final state than that for quarks.

M_H (GeV/c^2)	ϵ(hZ)	hZ($s\bar{s}$)	SM(no hZ)	observed
40	44.1	62.4	5.5	6
50	40.7	51.2	8.7	8
60	39.7	43.1	16.2	18
70	43.0	39.0	82.8	72
80	45.8	32.9	165.2	155
90	50.6	25.5	257.9	238
100	44.6	11.2	121.4	124
110	42.0	3.3	66.9	76

Table 3: The number of observed events compared to what is expected from background and signal ($H \rightarrow s\bar{s}$, assuming a SM-like cross section) for a few Higgs boson masses after a set of mass cuts to optimized to maximize the separating power for each tested Higgs mass.

Systematics

The estimation of the systematic uncertainties follows also closely the study done in the search for invisible Higgs decays[12]. Uncertainties in the background level that were taken into account were: the error on the luminosity, the choice of the jet clustering (replacing DURHAM by LUCLUS), the influence of the b-quark identification and the uncertainties in the Weν cross section. The combined effect from these uncertainites is different for each of the analyses and centre-of-mass energies, but they are around 1.4%, 2.2% and 1.8% for the low, intermediate and high mass analysis respectively. The shaking method, as described in [10, 12], has been also used in the analyses presented here. The effect on the background varies for the different years due to the usage of the different corrections. The uncertainties obtained by the shaking are in the range of 5.7% to 12.6% for the low mass, 6.2% to 10.2% for the intermediate mass range and 4.0% to 8.2% for the high mass range,

depending on the centre-of-mass energy. An overview of the systematic uncertainites on the background level are shown in Table 4, where the dominant contribution (the shaking method) is shown separately.

Analysis	year		
	1998	1999	2000
Low	10.1(10.0)	5.9(5.7)	12.7(12.6)
Intermediate	10.4(10.2)	6.9(6.2)	9.1(8.8)
High	8.3(8.2)	4.4(4.0)	7.3(7.1)

Table 4: Systematic uncertainties (in percent) on the background estimation for the different analyses in the different years of the LEP-2 period. The dominant contribution to the total uncertainty, obtained using the shaking method, is shown in parentheses.

The total systematic error on the signal efficiency coming from jet clustering, b-tagging and the shaking is between ± 1 to $\pm 3\%$ and the errors are the largest for the low mass analysis.

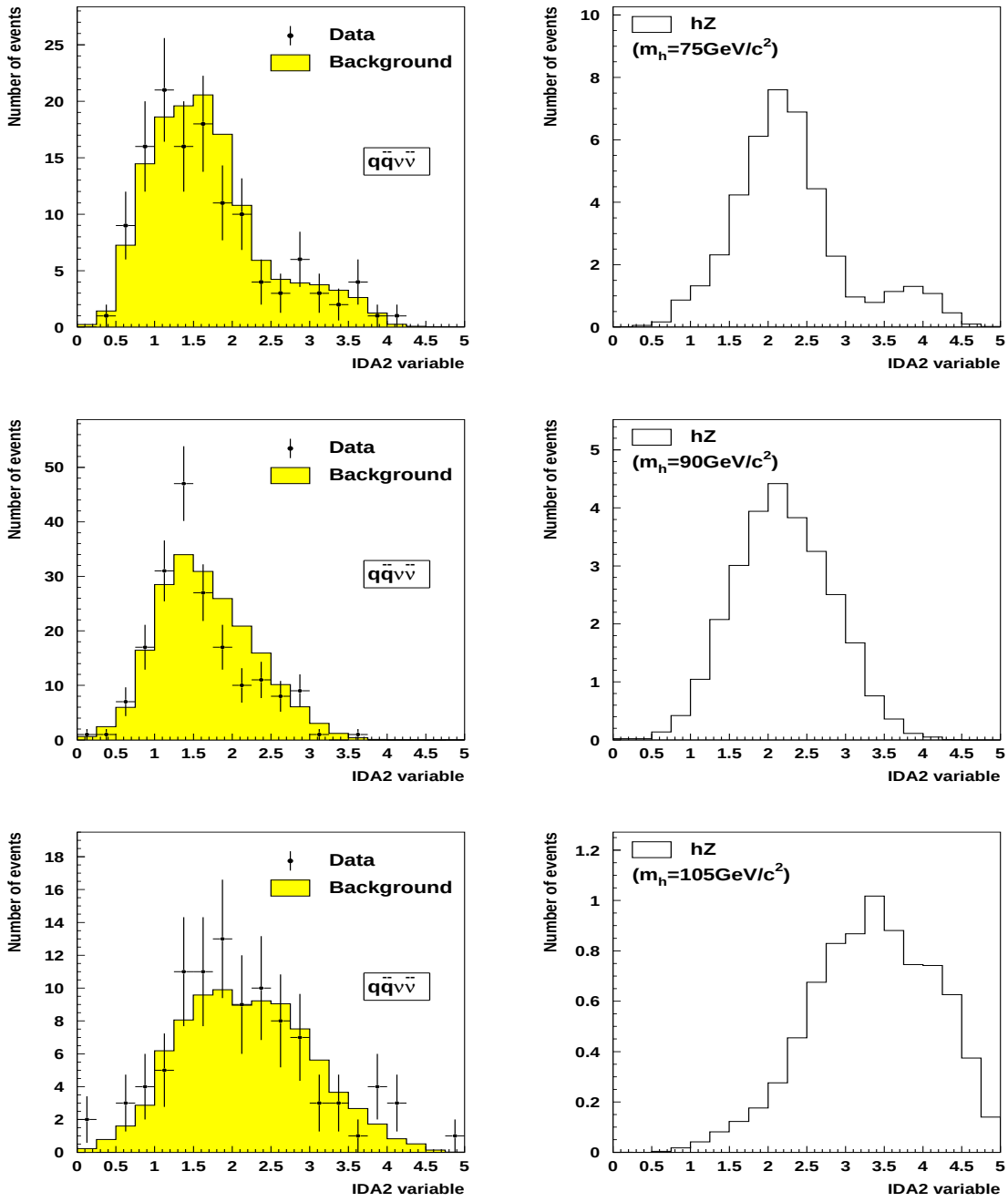

Figure 2: Distributions of the discriminant variables constructed to select hZ events (with the Higgs boson decaying into a pair of gluons) in the missing energy channel, obtained after a set of mass cuts optimized to maximize the separating power for each tested Higgs mass. The distributions shown here correspond to Higgs boson masses of 75, 90 and 105 GeV/c^2, with the data from all seven centre-of-mass energies combined. It has been shown that the signal purities in the bins of these variables are close to independent of the centre-of-mass energy, and that the evaluation can therefore be performed with moderate dilution using these combined distributions.

4.3 Jet(s) and missing energy (Low mass case)

The analysis used to measure the $Z\gamma^* \rightarrow q\bar{q}\nu\bar{\nu}$ cross sections[16] was adopted without major modifications to test the hypothesis of low mass ($m_h < 45$ GeV/c^2) Higgs boson production in the missing energy channel independent of the flavour of its decay products. After a pre-selection to reduce background events from $\gamma\gamma$, Bhabha and $Z\gamma$ background processes, three selections were designed, focussing on different expected topologies as a function of the mass of the Higgs boson.

The first selection was optimised to probe very low Higgs boson masses, using an explicit cut on the visible mass of the event, which was required to be below 6 GeV/c^2. The second selection exploited the large energy imbalance of $h\nu\bar{\nu}$ final states: events were split in two hemispheres according to the plane perpendicular to the direction of the thrust axis and required to have one of the hemispheres containing at least 99% of the total visible energy in the event. The third selection, which was less efficient at very low masses because of an explicit cut on the charged track multiplicity, was mainly based on a topological requirement: events were forced in a two jet configuration and an upper cut on the opening angle of the two jets was set at 78 degrees. All three selections used the information from the veto counters, by rejecting events with hits in veto counters far away from energy depositions in calorimeters or reconstructed tracks.

The three analyses were combined on an event-by-event basis, by selecting events that passed any of the three selections. The reconstructed visible mass spectra after passing at least one of the three selections are then combined in a single distribution that was used as the discriminant variable to test the various Higgs signal hypotheses. No specific mass cuts were applied for different test (Higgs) mass hypotheses. The most important background sources left were $Z\gamma^*$ and $We\nu$. The left plot in Figure 3 shows the number of events selected in data and in the simulation as a function of the reconstructed visible mass. Maximum Higgs signal efficiencies were around 65% and dropped to 40% for masses below 5 GeV/c^2 and above 40 GeV/c^{2}as can be seen in the right plot of Figure 3.

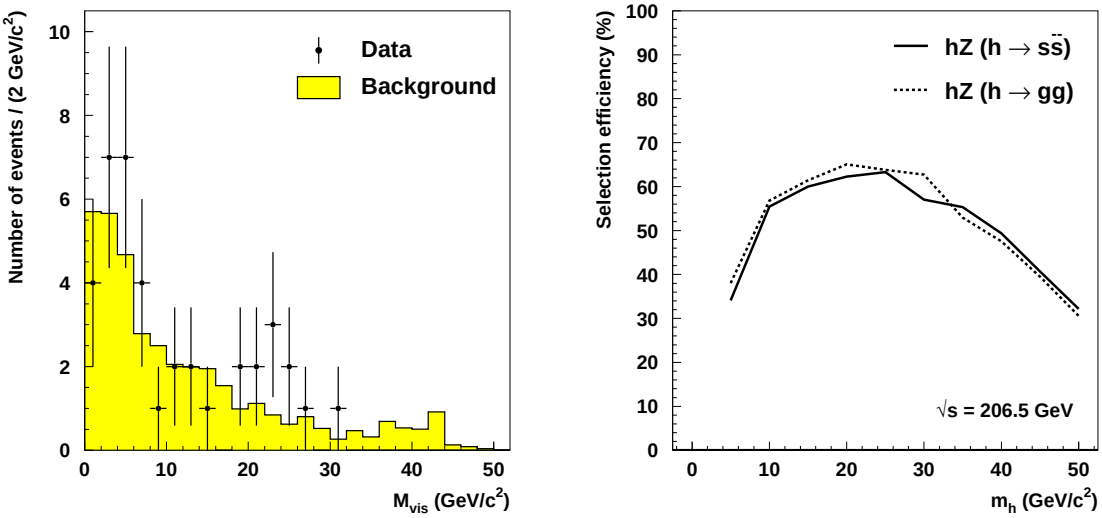

Figure 3: The left plot shows the distribution of the visible invariant mass of the hadronic system after the $q\bar{q}\nu\bar{\nu}$ event selection. The data are represented by the points, the expected background by the solid histogram. In the right plot the selection efficiency for Higgs signal events is shown as a function of the mass of the Higgs boson.

4.4 Two jets and a pair of isolated leptons

The $q\bar{q}e^+e^-$ and $q\bar{q}\mu^+\mu^-$ channels were analysed in the same way as in the $e^+e^- \rightarrow ZZ$, $Z\gamma^*$ production measurements[10, 16]. Events were selected by sequential cuts, initially without explicit condition on the invariant mass of the leptonic and hadronic system. The particle identification criteria were carefully tuned to maximise the efficiency of selecting leptons and the signal to background ratio. The final discriminate variable is the reconstructed hadronic mass and sets of mass cuts were applied to isolate the contribution from the hZ signal for each of the tested Higgs mass hypotheses, taking into account both the varying mass resolution of the signal and the changing background level from the ZZ and $Z\gamma^*$ processes that dominate these topologies.

The distribution of the reconstructed mass of one fermion pair when the mass of the second pair is within 15 GeV/c^2 of the Z mass is shown in Figure 5 for $q\bar{q}e^+e^-$ and $q\bar{q}\mu^+\mu^-$ separately. Signal efficiencies were evaluated for each Higgs mass and centre-of-mass energy for the $q\bar{q}e^+e^-$ and $q\bar{q}\mu^+\mu^-$ channels separately and were around 65% and 75% respectively. In Figure 4, the distribution of the LEP-2 'luminosity weighted' selection efficiency for both signals as a function of the mass of the Higgs boson is shown. To give an idea of the agreement between observation and expectation, at the final stage, in Table 5 the number of observed events in the muon analysis is compared to what is expected from background and signal ($H \rightarrow s\bar{s}$) for a few Higgs boson masses.

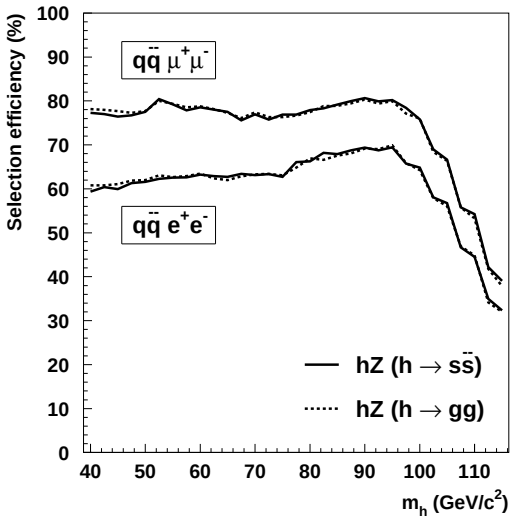

Figure 4: Distribution of the LEP-2 'luminosity weighted' selection efficiency for the $q\bar{q}e^+e^-$ and $q\bar{q}\mu^+\mu^-$ signal as a function of the mass of the Higgs boson. The solid(dashed) line respresents the processes in which the Higgs boson decays into $s\bar{s}$(a gluon pair).

M_H (GeV/c^2)	ϵ(hZ)	hZ($s\bar{s}$)	SM(no hZ)	observed
40	77.1	18.1	1.5	3
50	77.5	16.1	2.3	4
60	78.5	14.1	2.0	3
70	76.8	11.5	3.3	3
80	78.0	9.3	20.0	16
90	80.6	6.7	25.6	20
100	81.1	3.3	17.8	18
110	76.8	0.9	3.1	2

Table 5: Number of observed events with muons in the final state is compared to the expectation from background and signal (H $\rightarrow s\bar{s}$, assuming a SM-like cross section) for a few Higgs boson masses after a set of mass cuts to optimized to maximize the separating power for each tested Higgs mass.

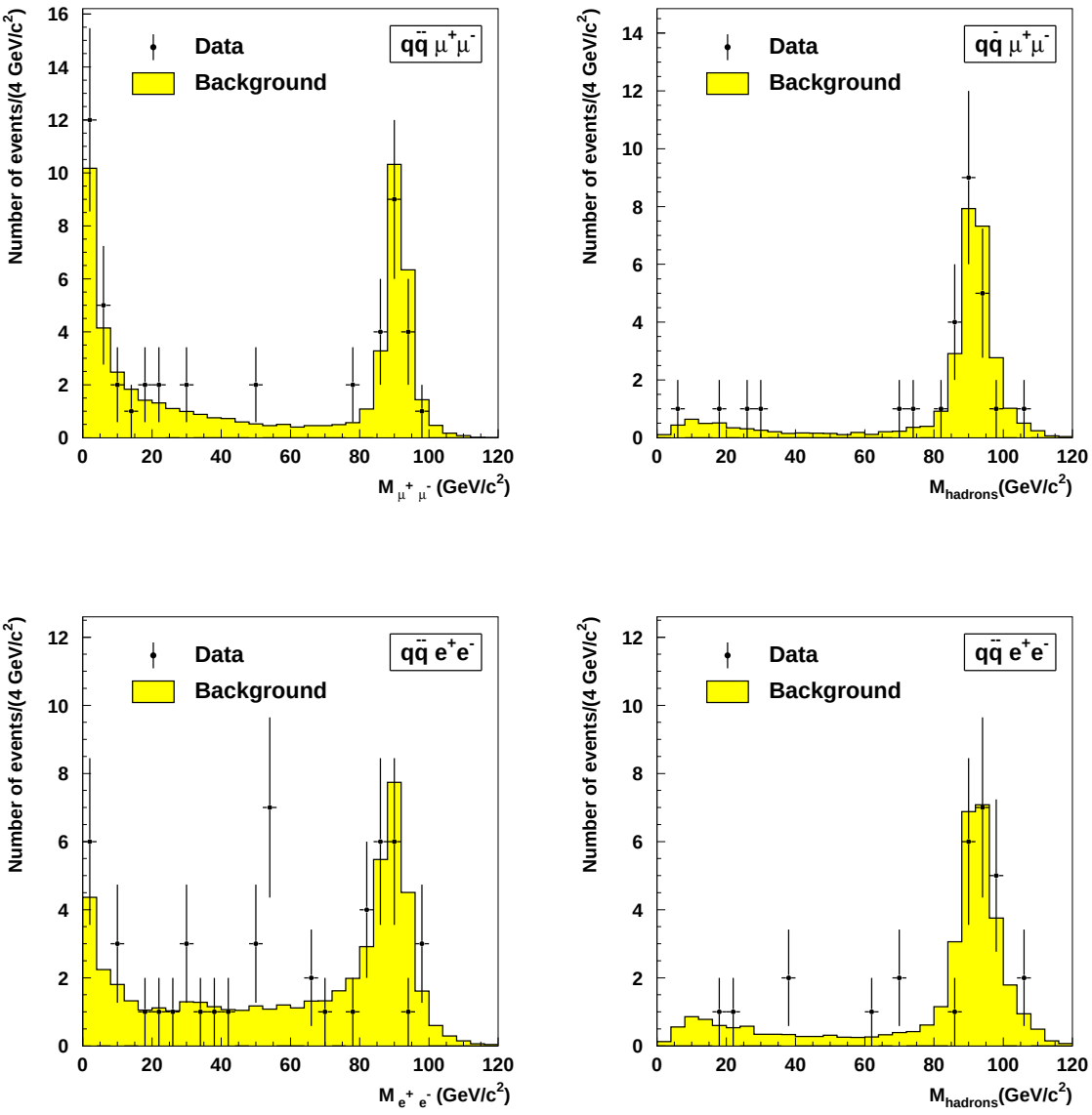

Figure 5: Distribution of the reconstructed mass in the $q\bar{q}l^+l^-$ channel of one fermion pair when the mass of the second pair is within 15 GeV/c^2 of the Z mass. The top left(right) plot shows the reconstructed mass of the di-lepton(hadronic) system in $q\bar{q}\mu^+\mu^-$ events. The lower two plots show the same for $q\bar{q}e^+e^-$ events.

5 Search for hA production

The search for hA production in the flavour blind hypothesis was designed to cover a large part of the kinematically accessible h and A mass range, and was based on general kinematic features such as event shapes and detailed mass information. Again, the significant higher multiplicity in gluon decays results in a higher selection efficiency for the gluon final state, but also leads to a worse mass resolution when compared to quark jets. To minimize biases that may arise from these competing effects, the (pre)selection efficiencies were determined using hA $\rightarrow$ light quarks samples, while the mass resolution was evaluated with hA $\rightarrow$ gluons samples.

5.1 Analysis streams

A first preselection was applied to all events, requiring them to have at least 20 charged tracks, a total reconstructed energy greater than 60% of the center-of-mass energy, and an effective centre-of-mass energy after initial state radiation greater than 150 GeV. The efficiencies of the multiplicity cut were typically 98% for the hA $\rightarrow$ light quarks signal samples, and 100% for the hA $\rightarrow$ gluons samples. In the rest of the analysis, it was necessary to consider separately three different topologies, to achieve good performance over a large range in the (m_h,m_A)-plane,as described below.

Four jets

Close to the kinematic limit and when both Higgs bosons have comparable masses, a four jet topology is expected. To analyse this topology, events were clustered into four jets with the Durham algorithm[17]. All jets were required to have an invariant mass larger than 2 GeV/c^2, and contain at least two charged particles. Events were retained in this stream if their thrust was below 0.85 and if the product of the smallest jet energy and inter-jet angle (called $E_{min}\alpha_{min}$) was greater than 10 GeV·rad. Dijet invariant mass information was used to reject events compatible with WW production as in [18], requiring the corresponding probability, called P_{WW}, to be less than 0.01. This proved helpful not only in the case of $m_h = m_A \sim$ 80 GeV/c^2 but also for other masses, where WW production contributes to the expected background through wrong jet pairings.

Three jets

With increasing mass difference between the h and the A, the events tend to become more three jet-like, since the decay jets of the lighter Higgs boson are not always resolved. The same behaviour is observed if h and A both have low masses, because of the larger boost in this case. To analyse this topology, only events with thrust values between 0.70 and 0.92 were kept. Events were first clustered into four jets, and the compatibility with WW production was then tested as in the four jet stream. The remaining events were clustered into three jets. As before, all jets were required to have a mass larger than 2 GeV/c^2 and to contain more than one charged particle.

Three jets with high thrust

Finally, if both Higgs bosons are very light (below 30 to 40 GeV/c^2), signal events tend to become cigar-like. Events were selected in this analysis stream if they had

a thrust ≥ 0.92, and were clustered into three jets, each jet having to satisfy the same quality criteria as above. As the dominant background comes from 2-quark processes the kinematic compatibility with a W-pair events does not need to be tested.

Distributions of the variables used (thrust, $E_{min}\alpha_{min}$ and P_{WW}) are shown in Figure 6 for the typical masses relevant to these three analysis streams. Their performances and complementarity are illustrated in Table 6, where typical mass-averaged efficiencies, obtained for the different categories of signal events, are summarised. The numbers of observed data and expected background events are shown in Table 7. At this stage the remaining flavour dependence was less than 2%.

	ϵ(4-jet)	ϵ(3-jet)	ϵ(high-thrust)
four-jet events	$\sim$ 70%	$\sim$ 45%	0- 5%
three-jet events	$\sim$ 50%	$\sim$ 70%	0- 5%
hight-thrust events	0-5%	0-5%	10-15%

Table 6: Efficiencies of the three analysis streams applied to three classes of signal events defined as follows: *Four-jet*: both m_h and $m_A > 60$ GeV/c^2; *high-thrust*: both m_h and $m_A < 30$ GeV/c^2; *three-jet*: remaining cases.

Centre of mass energy	189 GeV	196 GeV	200 GeV	>204.5 GeV
Four-jet stream :				
Expected background	433.5	221.3	259.0	634.5
Observed events	459	248	232	642
Three-jet stream :				
Expected background	1593.3	750.6	797.0	1894.3
Observed events	1585	736	772	1824
High-thrust stream :				
Expected background	1384.9	642.5	654.3	1516.3
Observed events	1331	612	607	1450

Table 7: Numbers of observed and expected background events for all data sets considered and for the three analysis streams.

5.1.1 Final discriminant

In all three analysis streams, a four-constraint fit was performed on the events, requiring total energy and momentum conservation. A discriminant variable was then built from the reconstructed jet and dijet masses and their errors, by minimising the following quantity:

$$\chi^2(m_{1,test}, m_{2,test}) = \left[\left(\frac{|m_{1,rec} - m_{1,test}|}{\delta m_{1,rec}} \right)^2 + \left(\frac{|m_{2,rec} - m_{2,test}|}{\delta m_{2,rec}} \right)^2 \right],$$

defined for each event, over all available pairing combinations. In the above expression, $m_{1,rec}$ is the mass of a given dijet, $m_{2,rec}$ is the mass of the opposite dijet in the four-jet stream, and of the opposite jet in the other streams, and $\delta m_{1,2}$ are the corresponding

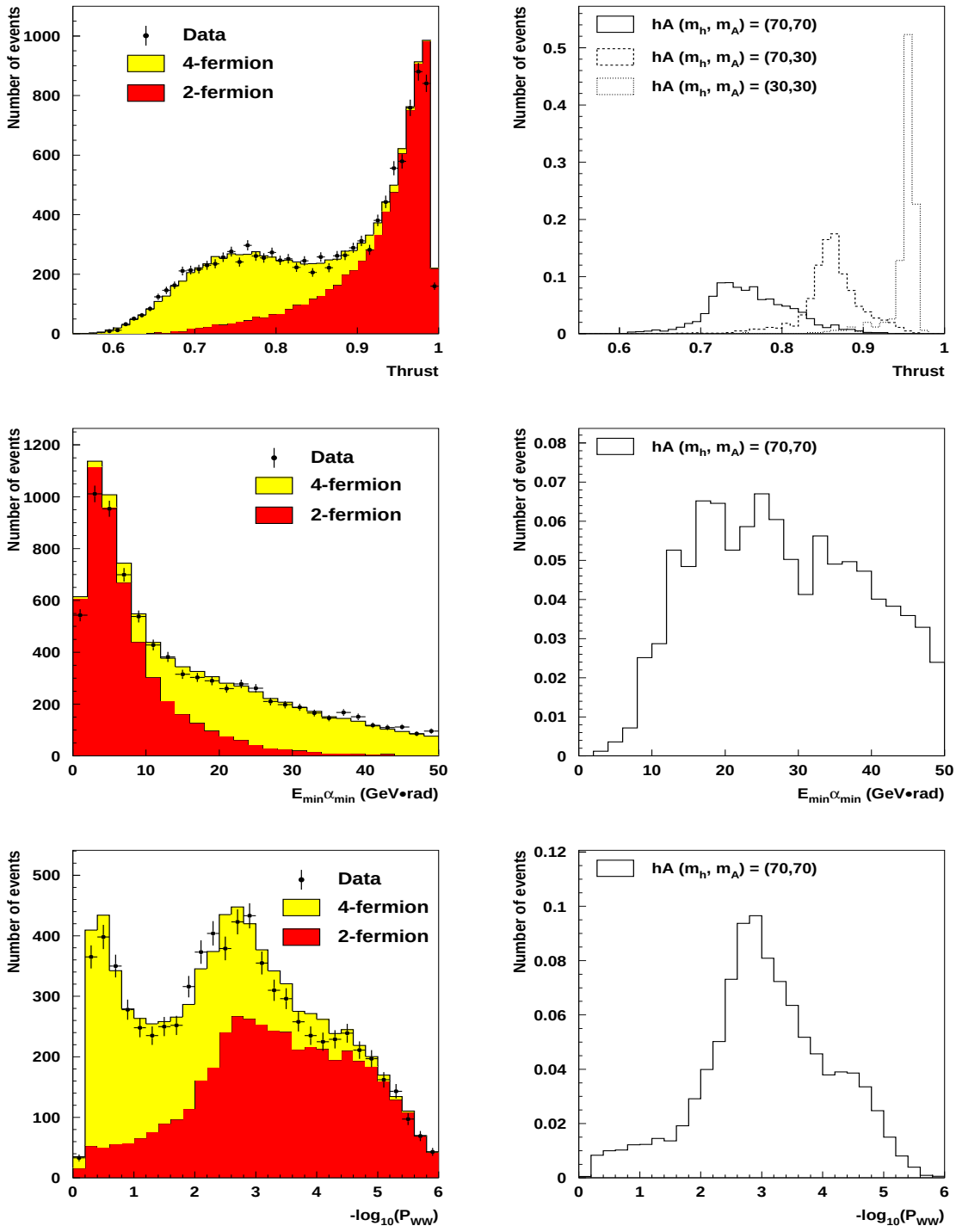

Figure 6: hA search: data to Monte-Carlo comparisons for the variables used in the three selection streams. On the right part, the dots represent the data, the light(dark) histogram corresponds to the expected 4-fermion(2-fermion) background. The discriminating power is indicated by showing the distributions from representative signal samples.

errors. This discriminant variable was computed for data and background, for each test

mass configuration ($m_{1,test}, m_{2,test}$), on a 1×1 GeV/c^2 grid in the (m_h,m_A)-plane and projected into histograms as illustrated in Figure 7. The range and bin size of the histograms is the same for all analysis streams and mass configurations.These histograms were used for the statistical evaluation of the compatibility of the data with the simulation, following the procedure described in [19].

To determine the shape of the signal distributions at mass configurations that were not simulated, the histograms were linearly interpolated, bin by bin, between the three closest simulated points. This procedure is adapted in this particular case, because the discriminant was designed to have a slowly varying distribution for the signal, as a function the signal mass. The validity of this procedure is shown in section 5.2.

The three-jet stream and the high-thrust stream are statistically independent and were combined. The overlap between these selections and the four-jet stream was solved at this stage by choosing the best solution for each mass point, based on the expected performance.

5.2 Systematic uncertainties

The comparison between the predicted Standard Model background rates and the number of observed events after the selections described above leads to an estimated systematic uncertainty on the backgrounds of 5% in the four-jet and three-jet streams, and 10% in the high-thrust stream.

As stated earlier, the flavour dependence of the selection efficiencies was estimated by comparing the results obtained for gluon decays, light quark decays, and b-quark decays. The preselection efficiency is slightly worse in the case of quark decays, and is applied to the gluon decays as well. The remaining selections have a flavour dependence of less than 2%. This number is taken as a contribution to the systematic uncertainty on the signal rate.

An example for the signal interpolation is shown in the left plot of Figure 8. The discriminant distribution for mass configuration (110,40) as obtained from simulation is compared to an interpolation between two neighbouring simulated mass points, namely (110,30) and (110,50). The shapes are well reproduced. To quantify more precisely what accuracy can be expected from this procedure, the previous exercise was repeated on a large number of simulated mass configurations. In each case, the bin contents of the simulated and interpolated histograms were compared. The distribution has a spread of 5% which is taken as a second contribution to the systematic uncertainty on the signal rate. Note that this is a conservative estimate as the real interpolation is over smaller intervals, since the simulation is done every 10×10 GeV/c^2.

Finally, the right plot of Figure 8 shows the distribution of the discriminant variable obtained for quarks and gluons, at the mass point (110,30). As expected, a worse mass resolution on gluon jets translates into a somewhat reduced discriminating power (this is true for all mass points). The present analysis, with a preselection determined on light-quark signal samples, and a kinematic analysis calibrated on gluon samples, thus has no bias towards given flavour that would invalidate the results when considering other hadronic decays of the Higgs bosons.

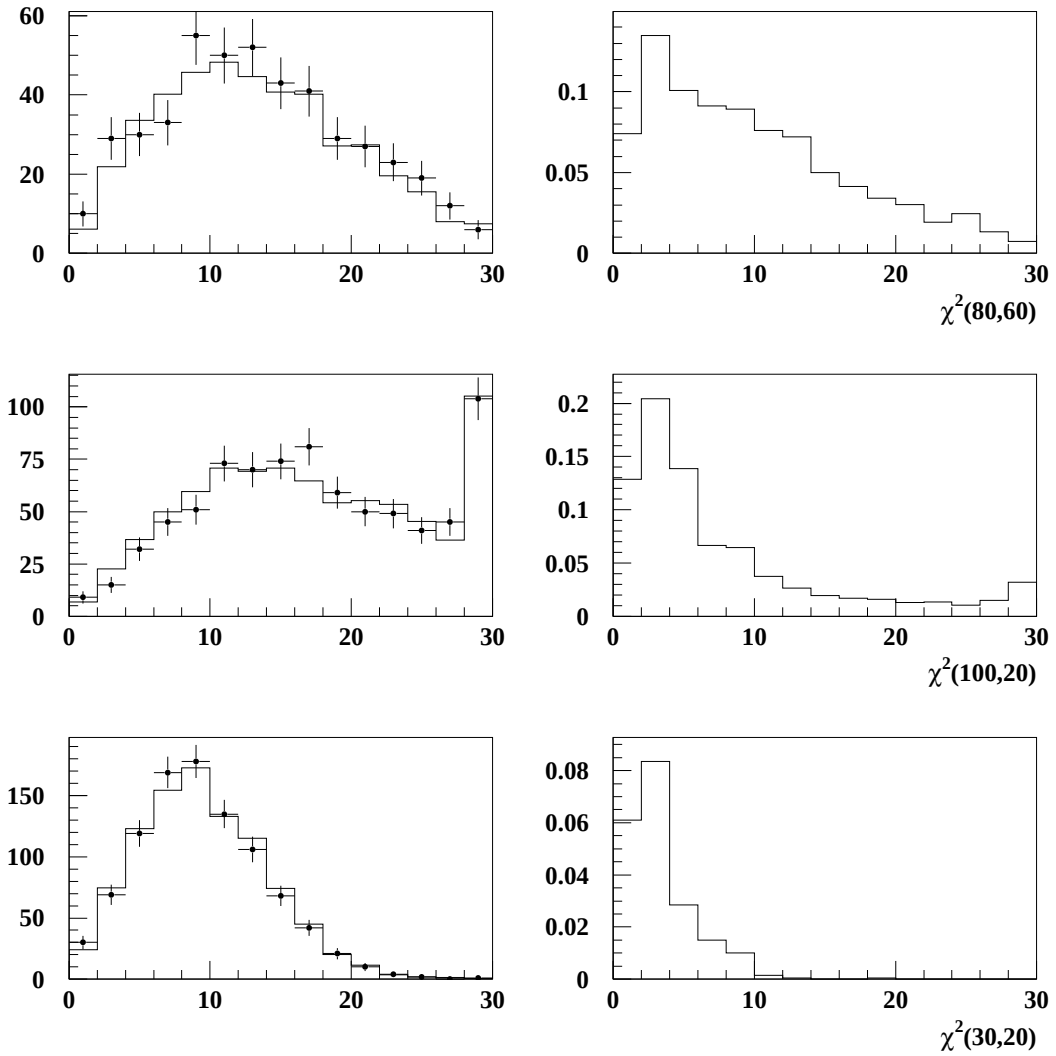

Figure 7: hA search: distributions of the variable $\chi^2(m_1, m_2)$ for the data and expected background (left) and signals (right). The upper plots show the discrimination obtained for a (m_h,m_A) = (80,70) hypothesis in the four-jet stream. The central plots show the discrimination obtained for a (m_h,m_A) = (100,20) hypothesis, in the three-jet stream. The lower plots show the discrimination obtained for a (m_h,m_A) = (30,20) hypothesis, in the high-thrust stream.

6 Results

Results from the different analyses and topologies have been combined, and the statistical compatibility with a possible Higgs signal has been evaluated using the likelihood ratio technique[19] that was also used in the search for the Standard Model Higgs boson[20]. No evidence for a signal production has been observed and results are presented in terms of excluded cross sections as a function of the Higgs mass. The results will be presented for hZ production and for hA production separately.

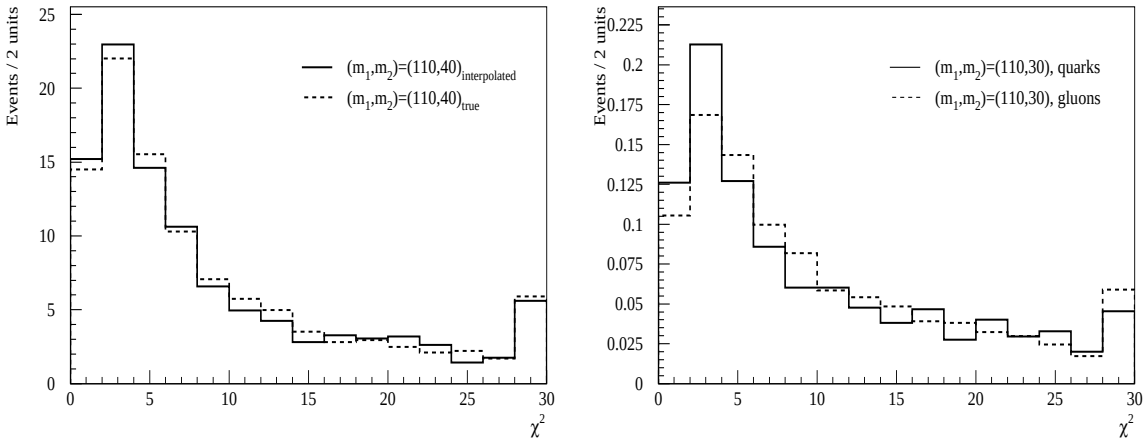

Figure 8: The left plot shows with the solid line χ^2 distribution for the compatibility with a (110,40) mass hypothesis when interpolation from the nearest simulated samples at (110,30) and (110,50) GeV/c^2. It is compared with the 'true' (dashed line) distribution from a simulated sample at (110,40). The right plot shows the same distribution for two different simulated samples: a Higgs decaying into either $s\bar{s}$ (solid line) or gg (dashed line) to indicate the worse mass resolution for a purely gluonic final state.

6.1 Excluded cross sections for hZ production

The strategy to obtain cross section exclusions independent of the flavour of the hadronic Higgs decay was to use systematically the most conservative result. Cross section limits were calculated for Higgs decays in either gluon or $s\bar{s}$ pairs. For masses above 40 GeV/c^2 the results obtained from the $s\bar{s}$ final state are always the most conservative. The transition between the hZ fully hadronic and the hA 3-jet analysis and between the two missing energy channels was done at m_h=40 GeV/c^2, a mass where the performance of these channels is similar. In Figure 9 the excluded cross section for a Higgs boson with purely hadronic decays is shown, normalised to the SM cross section. Observed and expected limits agree well over a wide range of masses. The largest discrepancy occurs for a Higgs mass around 30 GeV/c^2 where an excess $\sim 2.5\ \sigma$ is observed.

In Table 8 the mass limits obtained for a Higgs boson with SM production cross section and exclusively decaying into either $s\bar{s}$ or gg are compared to the results of the SM Higgs search.

	expected lower limit	observed lower limit
DELPHI (H$\rightarrow s\bar{s}$)	108.0	110.6
DELPHI (H$\rightarrow$ gg)	109.2	111.0
DELPHI (SM decay)[20]	113.3	114.1

Table 8: The expected and observed sensitivity (in GeV/c^2) for the mass of a hadronically decaying Higgs boson assuming its cross section is identical to that in the SM in comparison with the results of the SM Higgs search.

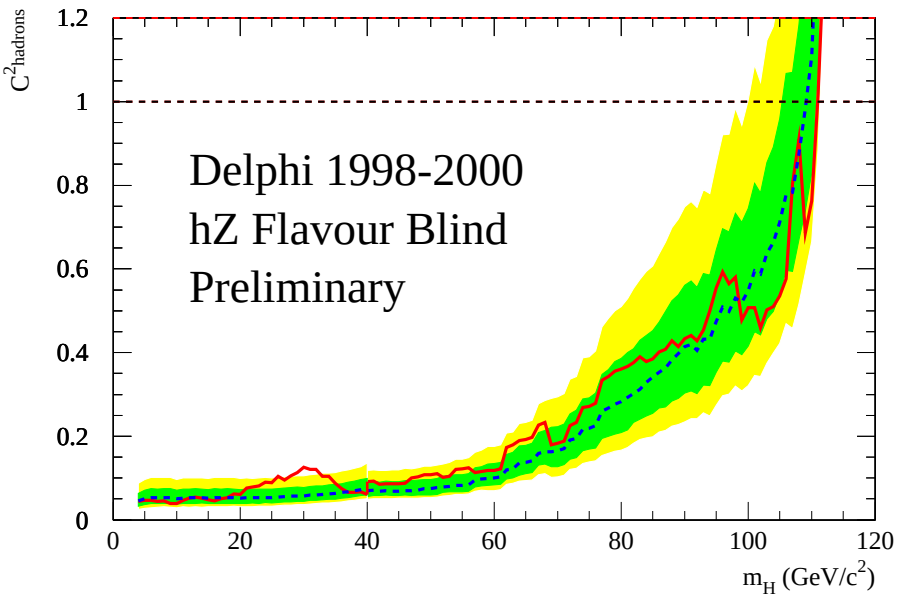

Figure 9: Excluded hZ cross section relative to that of the SM Higgs boson as a function of the Higgs boson mass in case the Higgs boson is decaying hadronically. Curves are the observed (solid) and expected median (dashed) excluded cross sections, while the bands correspond to the 68.3% and 95% confidence intervals.

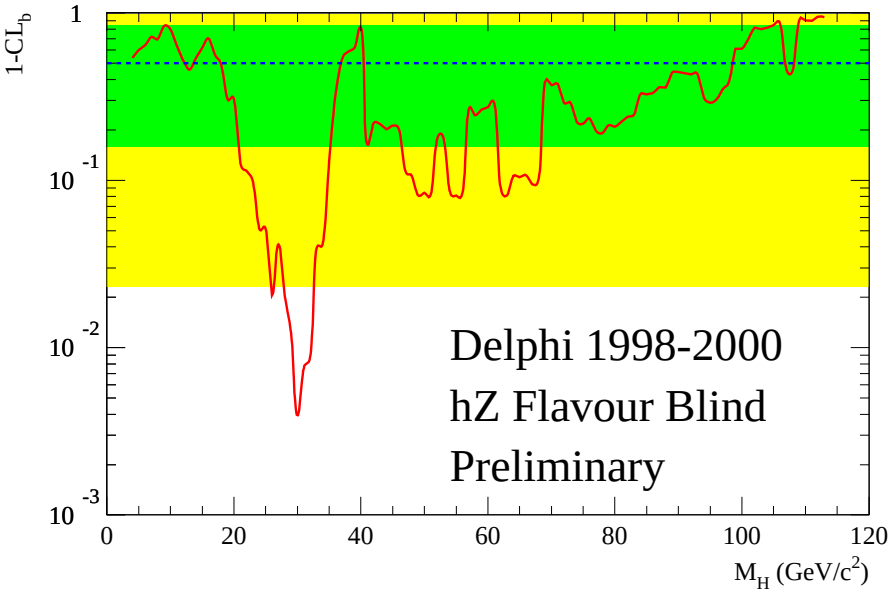

Figure 10: Confidence levels in the background hypothesis as a function of the Higgs boson mass, computed with the likelihood ratio technique[19]. Curves are the observed (solid) and expected median (dashed) confidences from background-only experiments, while the bands correspond to 68.3% and 95% confidence intervals from the background-only experiments.

6.2 Excluded cross sections for hA production

The three different hA analysis streams were combined to search for Higgs boson pair production. No evidence for signal was observed. Figure 11 displays the results in the (m_h,m_A)-plane. The excluded cross-sections are given in terms of a factor C^2, which equals 1 when the cross-section is equal to the maximal value allowed by electroweak symmetry breaking and when the branching fraction into hadronic final states is 100%.

When both Higgs boson masses are similar and when the production cross-section is maximal, the region below m_h+m_A∼140 GeV/c^2 is excluded. When one of the Higgs boson is very light, the opposite one is constrained to lie outside the region limited by 4 GeV/c^2 and 100 GeV/c^2. The 3-jet and high-thrust analysis streams allow a significant portion of the mass plane to be excluded even when the production cross-section is smaller than 25% of the maximal rate.

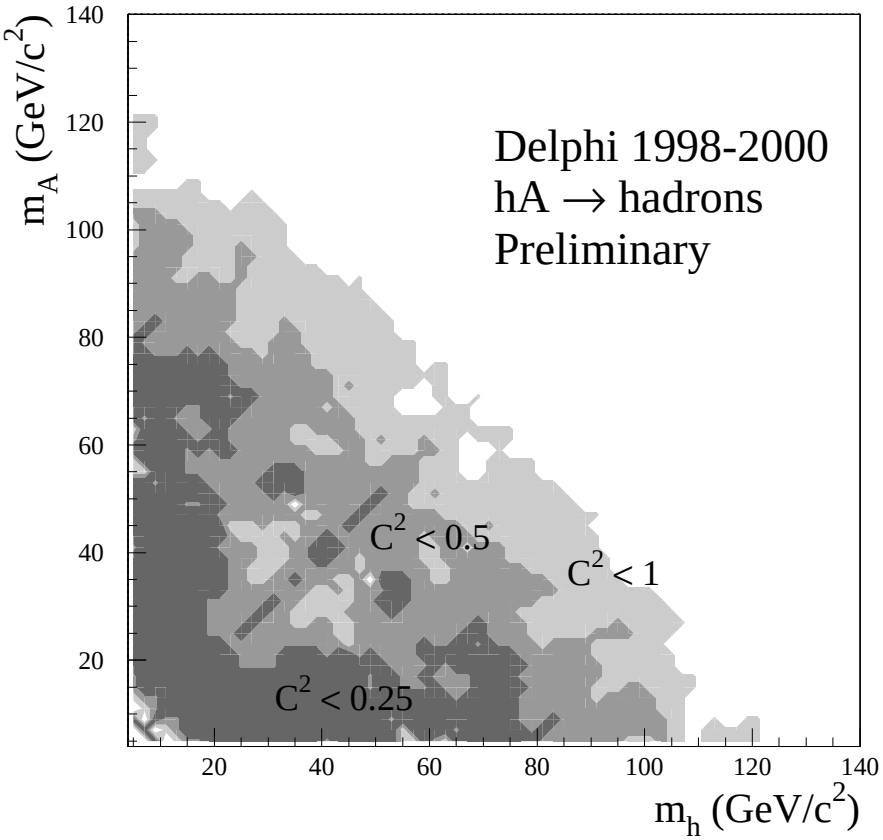

Figure 11: Excluded cross sections in the (m_h,m_A)-plane, in terms of a factor C^2, which equals 1 when the cross-section is equal to the maximal value allowed by electroweak symmetry breaking and when the branching fraction into hadronic final states is 100%.

7 Summary

DELPHI has used LEP-2 data to search for hadronically decaying Higgs bosons independently of the flavour of the decay products. No signal was found in either of the two main

production mechanisms ($e^+e^- \to Z^* \to hZ$ and $e^+e^- \to Z^* \to hA$) studied, in a broad range of masses extending from 4 GeV/c^2 to close to the kinematic limit.

For the hZ process, cross-sections larger than about 10-60% of the expected standard model values were excluded in the range of masses from 4 to 100 GeV/c^2, independent of the flavour of the Higgs boson decays. In the assumption of a production cross-section equal to that of the standard model, lower observed and expected mass limits of 108.0 GeV/c^2 and 110.6 GeV/c^2 were obtained, respectively.

For the hA process, a large part of the available mass range was excluded, extending roughly from $m_{h,A}$= 4 GeV/c^2 to $m_{h,A}$ = 120 GeV/c^2 (for m_h+m_A<120 GeV/c^2), independent of the flavour of the Higgs boson decays, in the assumption of production cross-sections equal to the maximum value allowed by electroweak symmetry breaking.

References

[1] J. F. Gunion, H. E Haber, G. L. Kane and S. Dawson The Higgs Hunter's Guide, Addison-Wesley Publishing Company, 1990

[2] M. Carena, S. Heinemeyer, C. E. Wagner and G. Weiglein, Suggestions for improved benchmark scenarios for Higgs-boson searches at LEP2, hep-ph/9912223.
M. Carena, S. Mrenna and C. E. Wagner, Phys. Rev. D **60** (1999) 075010
W. Loinaz and J. D. Wells, Phys. Lett. B **445** (1998) 178
M. Carena, J. Ellis, A. Pilaftsis, C. E. Wagner Nucl. Phys. **B586** (2000) 92

[3] X. Calmet and H. Fritzsch, *Phys. Lett.* **B496** (2000) 190.

[4] DELPHI Collaboration (P. Abreu *et al.*) *Nucl. Instr. and Meth.* **378** (1996) 57.

[5] S. Jadach, B. F. Ward and Z. Was, *Comp. Phys. Comm.* **130** (2000) 260.

[6] T. Sjöstrand, *Comp. Phys. Comm.* **39** (86) 347; *Comp. Phys. Comm.* **82** (94) 74.

[7] E. Accomando and A. Ballestrero, *Comp. Phys. Comm.* **99** (1997) 270.

[8] F. A. Berends, R. Pittau and R. Kleiss *Comp. Phys. Comm.* **85** (1995) 437.

[9] P. Janot, in CERN Report 96-01, Vol. 2, p. 309.

[10] DELPHI Collaboration, P. Abreu *et al.*
ZZ production in e^+e^- interactions at sqrt(s) = 183 - 209 GeV
CERN-EP/2003-009 (Submitted to Eur.Phys. J. C)

[11] A. Ballestrero *et al.*, CERN-EP/2000-009 (2000), 137

[12] DELPHI Collaboration, P. Abreu *et al.*,
Searches for invisibly decaying Higgs bosons with the DELPHI detector at LEP
(To be submitted to Eur. Phys. J. C)

[13] T.G.M. Malmgren, *Comp. Phys. Comm.* **106** (97) 230;
T.G.M. Malmgren and K.E. Johansson, *Nucl. Instr. and Meth.* **403** (1998) 481.

[14] G.C. Fox and S. Wolfram, *Nucl. Phys.* **B149** (1979) 413

[15] DELPHI Collaboration, P. Abreu *et al.*
b-tagging in DELPHI at LEP
CERN-EP/2002-088 (Submitted to Eur.Phys. J. C)

[16] DELPHI Collaboration, P. Abreu *et al.*
Z/γ^* production in e^+ e^+e^- interactions at $\sqrt{(}s)$ = 183-209 GeV
(To be submitted to Eur.Phys. J. C)

[17] S. Catani, Yu.L. Dokshitzer, M. Olsson, G. Turnock, B.R. Webber Phys. Lett. B **269** (1991) 432
N. Brown, W. Stirling, Zeit. Phys C53(92) 629

[18] I. Van Vulpen and N. Kjær, DELPHI 99-169 PHYS 839 (1999).

[19] A. L. Read, in CERN Report 2000-005, p. 81 (2000).

[20] DELPHI Collaboration, P. Abreu *et al.*
Search for the Standard Model Higgs Boson at LEP
CERN-EP/2003-008 (Submitted to Eur. Phys. J. C)